Optimization of hemispherical electrostatic analyzer manufacturing with respect to resolution requirements

J. H. Vilppola, J. T. Keisala, and P. J. Tanskanen
University of Oulu, Department of Physics, Oulu, SF-90570, Finland

H. Huomo
VTT Technical Research Centre of Finland, Instrument Laboratory, Espoo, SF-02151 P.O. Box 107, Finland

(Received 7 December 1992; accepted for publication 23 April 1993)

Electrostatic analyzers with different geometries have been used extensively in space plasma investigations. When the energy resolution requirements are such that $\Delta E/E \approx 10\%$ the instrument is rather simple to design and to manufacture. However, when an energy resolution of $\approx 1\%$ is required, the manufacturing costs increase rapidly. For analyzers with an energy resolution of $\approx 10\%$ the calibration can also be used to correct for manufacturing errors when they appear. In this paper, it has been shown that to reach an energy resolution $\Delta E/E = (1.6 \pm 0.2)\%$ using a hemispherical electrostatic analyzer with outer and inner radii 101.25 and 98.75 mm respectively and plate thickness 0.4 mm, an accuracy of 25 μm in the alignment of one hemisphere with respect to the other is sufficient. It is also shown that the effect on the energy resolution of an indentation of the surface of one of the conductors can be neglected as long as its depth is less than ≈ 100 μm. Larger indentations can easily be detected in the manufacturing process. For each case considered, the maximum permitted loss of transmitted particles with respect to the transmission of an ideal instrument has been defined as 10%. Similarly, it has been specified that the deviations in the distributions of entrance angles of transmitted particles shall be less than 0.1°.

I. INTRODUCTION

Cassini is a NASA planetary mission planned to be launched in 1997. The primary goal of the mission is to study Saturn's plasma environment, where the satellite is planned to arrive in 2004. The Cassini mission includes space plasma investigations[1] in Saturn's magnetosphere as well as studies of planetological phenomena such as the atmospheres of Saturn and Titan and the surfaces of the icy satellites and rings. Secondary objectives include investigations of the solar wind and interstellar ion pickup.

Different space-plasma diagnostic instruments are used for this mission.[2] One of the plasma sensors is the ion beam spectrometer (IBS), which is a single hemispherical electrostatic analyzer with three fan-shaped entrance windows for incoming charged particles. Channel electron multipliers (CEM) are used as detectors in the IBS instrument.[3] The desired energy resolution for observed ions has been set to $\Delta E/E = (1.6 \pm 0.2)\%$, and the maximum loss of transmitted particles with respect to the transmission of an ideal instrument has been defined as 10%. Similarly, it has been specified that the deviations in the distributions of entrance angles of transmitted particles should be less than 0.1°. In order to optimize the manufacturing costs, the goal of this investigation was to calculate the upper limits of the geometrical tolerances of the IBS instrument for which fixed baseline dimensions and specifications had been given.

This paper presents a calculation method that describes the performance of the IBS instrument and how the influence of the geometrical manufacturing and assembly errors can be estimated. In particular, the misalignment of the hemispheres has been considered carefully. Section II gives the theory and algorithms used for these purposes, in Sec. III we present the results, and Sec. IV includes discussions of the results.

II. THEORY AND ALGORITHMS

In an ideal case, IBS is simply a hemispherical condenser with a voltage applied between the hemispheres. Solving Gauss' law leads to an equation where the electric field E is given as a function of radius r,[4,5] which can be written

$$E = \frac{\Delta U}{r^2}\left(\frac{R_1 R_2}{R_2 - R_1}\right). \tag{1}$$

The equations of motion in a central force field can be written for the charged particle inside the ideal IBS sensor by using spherical polar coordinates shown in Fig. 1 and the planar condition by choosing $\phi = 0$.[6]

$$m\ddot{r} - mr\dot{\theta}^2 + \frac{k}{r^2} = 0, \tag{2}$$

$$2mr\dot{r}\dot{\theta} + mr^2\ddot{\theta} = \frac{d}{dt}(mr^2\dot{\theta}) = 0, \tag{3}$$

where

 0034-6748/93/64(8)/2190/5/$6.00

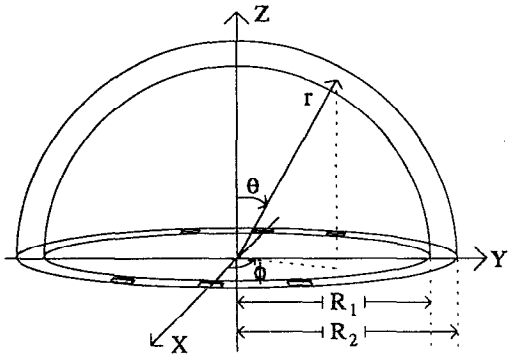

FIG. 1. Coordinate systems and parameters of the IBS instrument.

$$k=Q\Delta U\left(\frac{R_1R_2}{R_2-R_1}\right). \tag{4}$$

These differential equations can easily be solved analytically and the solutions are Kepler's elliptical orbits. In our case, these orbits cannot be used since spherical symmetry is broken immediately when geometrical manufacturing or assembly errors occur. These cause the constant k of Eq. (4) to become a function of distance between the shells ($\Delta R=R_2-R_1$). Equations (2) and (3) then no longer yield elliptical orbits and have to be solved numerically. For our purposes the fourth-order Runge–Kutta method was used to obtain solutions.[7]

If the constant k is allowed to change, Eqs. (2) and (3) will only yield an approximate solution for the radial component of the electric field. For example, breaking the spherical symmetry through erroneously positioned ideal hemispheres would yield a tangential electric field component. This component is very small as can be seen by considering the misalignment of the centers of the two hemispherical conductors of radii 101.25 and 98.75 mm by 25 μm along one of the major axes in an orthogonal coordinate system. In this coordinate system the tangential component has its maximum value in the space between the hemispheres directly above the centers. An approximate value for the ratio of the tangential field component to the radial component is 2.5×10^{-4}. Thus, it can be assumed (a) that a possible 25 μm misalignment of the two hemispheres would mostly affect the radial component, (b) that Eqs. (2), (3), and (4) can be used just as in an ideal case, and (c) that the planar condition ($\phi=0$) is applicable. Three-dimensional solutions can easily be calculated by using coordinate transformations.

Equation (5) shows that only the separation of the hemispheres (ΔR) can influence the motion of the ions. In nonideal cases, ΔR has to be known as a function of coordinates r, θ, and ϕ (see Fig. 1) so that the differential equations of motion can be solved. This can be carried out by solving a three-dimensional geometrical problem analytically when possible, or simply by constructing a three-dimensional matrix from which the local value of the distance can be read when needed.

The theory described above can be used with Monte Carlo simulation[7] where random values are given to parameters describing the ions incident on the IBS apertures. These parameters are the kinetic energy of the ion, position of the incoming particle with respect to the entrance aperture, and the two angular parameters which define the initial direction of the velocity vector (see Fig. 2). Using these values the trajectories can be solved and the fraction of the transmitted ions can be found as a function of the geometrical imperfections of the IBS sensor.

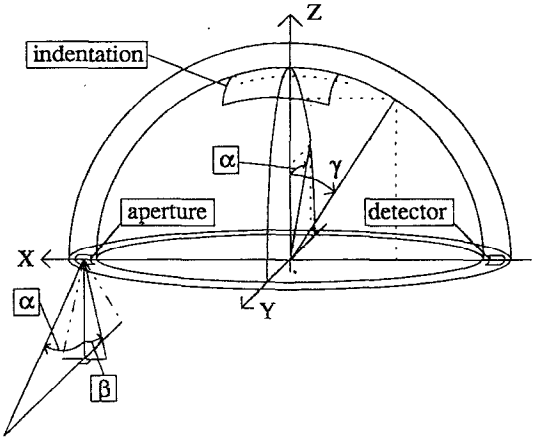

FIG. 2. Angular variables used for the initial speed vector and for the indentation as appearing in the IBS instrument.

When random values are given to the parameters, the following points should be considered. First, the distributions of angular variables α and β in Fig. 2 have the form of a cosine function. This means that ions "see" a smaller aperture when angular parameters have high values. This gives a pronounced effect especially on the angle α which has a very large range. Second, the kinetic energy of the ion is affected by stray electric fields outside the IBS. This effect can be taken care of by calculating the potential difference between the entrance location of the ion and the center of the aperture. Naturally, the ion obtains more kinetic energy near the inner hemisphere and loses it near the outer hemisphere. This stray field is defined by actual aperture geometry of the instrument front plate and is not affected by the shape or misalignment of the hemispheres. Thus, the effects of the stray field on the angular acceptance are not considered here.

III. RESULTS

A program was developed to investigate the effect of misalignment of the hemispheres as well as the effect of a single indentation on the surface of the inner hemisphere. (The program also aids investigation of the ideal instrument with numerical methods instead of analytical ones.[8])

In order for the results given by the program to be easily interpretable, only a single aperture (along the x axis) was used (see Figs. 1 and 2). Actually the aperture used in the calculations was differential in the y direction, contrary to the real geometry shown in Fig. 1. If the real geometry of the aperture is taken into account a mixing of angles α and β defined in Fig. 2 would occur due to the

TABLE I. Values of parameters used in the calculations.

Nominal kinetic energy (E_0)	100 eV
Energy range (of nominal)	±3%
Range of α	±75%
Range of β	±3°
Inner radius (R_1)	98.75 mm
Outer radius (R_2)	101.25 mm

curved shape of the aperture. This "butterfly" effect is elaborated in detail in Ref. 8. Table I shows the values of the parameters used in the calculations. The misalignment of the hemispheres in the direction of each coordinate axis is defined separately. This allows investigation of misalignments in every possible direction. The depth of the indentation was also adjustable and the other dimensions were chosen so that the extensions of the indentation was ±10° in α and γ (see Fig. 2). The voltage applied between the hemispheres was chosen so that ions with a given nominal kinetic energy had a circular trajectory in the middle of the hemispheres. In the calculations of affects caused by misalignment, the coordinate axes were chosen so that the inner hemisphere was moved with respect to the outer hemisphere. Protons were used as incoming ions. For an electrostatic instrument the behavior is identical for all ions with the same energy/charge (E/Q) ratio.

The influence of misalignment was studied in the direction of the main coordinate axes (see Figs. 1 and 2). In each of three directions, the results were calculated for misalignments ranging from 0 to 120 μm in steps of 5 μm. One million protons were injected in each case and the

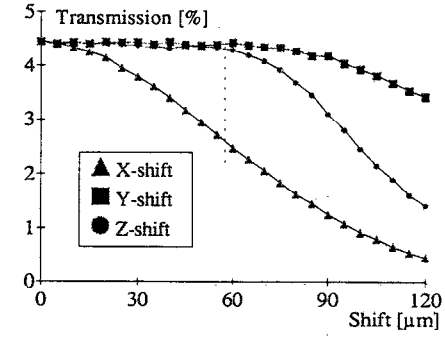

FIG. 3. The transmission percentage as a function of shifts in x,y, and z directions is shown. If the y- or z-direction shifts exceed 60 μm (indicated by the dashed line), the transmitted particles spill outside the allowed energy range of ±3% (see Fig. 5) and the actual transmission losses are smaller than those indicated in this figure. This effect is not present in the x-shift calculations.

transmission percentage calculated. The transmission percentages as functions of displacement are shown in Fig. 3. The transmitted protons were categorized in terms of their kinetic energy and the angles α and β. The energy distributions of the transmitted particles in the ideal case and for a 60 μm misalignment in each direction are shown in Fig. 4 as are the distributions of the initial angles of the transmitted particles. Distributions give the number of transmitted particles per bin for angle α divided by the value of cos α. The distributions of the 60 μm misalignments show the typical effects for each direction. The full width at half maximum (FWHM) values, the average of the energy E

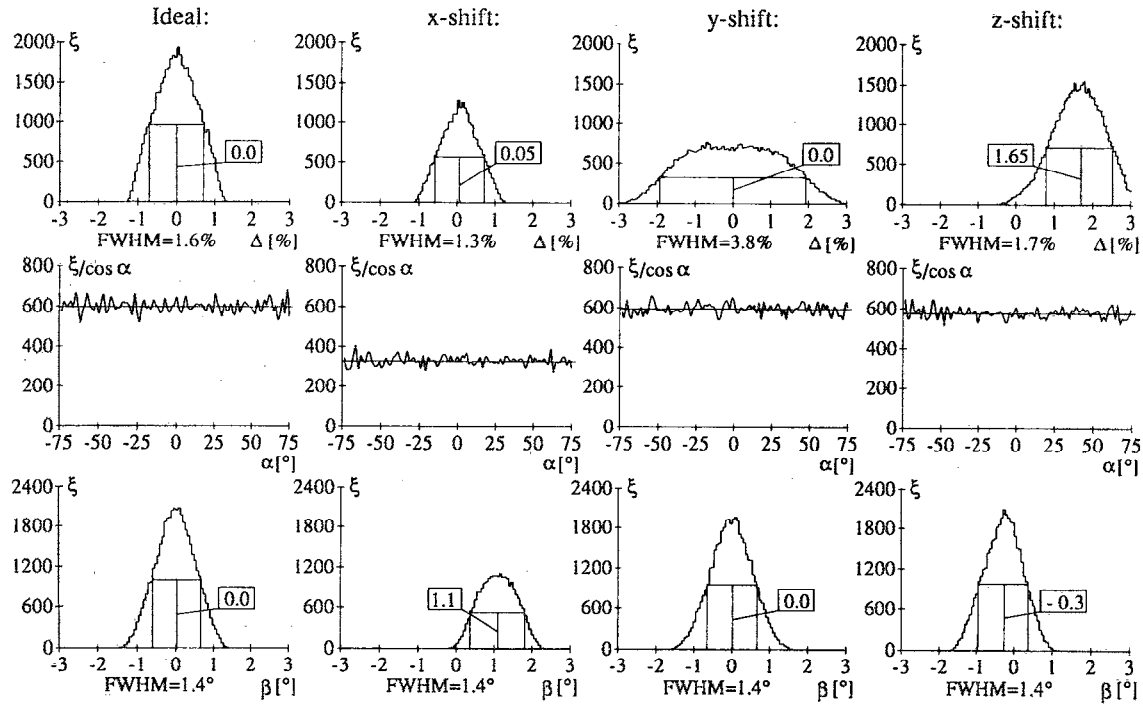

FIG. 4. The energy distributions and the distributions of the angles α and β in an ideal case and in cases when a 60 μm misalignment in either x,y, or z direction has occurred. The full width at half maximum (FWHM) values and the average of the distributions are shown for the energy and angle β distributions. $\Delta=(E-E_0)/E_0$, where E_0 is the nominal kinetic energy. ξ=number of transmitted particles per bin. In the angle α distributions the ξ values are divided by the value of cos α in order that the changes of the distributions become easily perceptible. The bin widths are $\delta E=0.06\%$, $\delta\alpha=1.5°$, and $\delta\beta=0.06°$.

TABLE II. The full width at half maximum (FWHM) values, the average of the energy E and angle β distributions, and transmission percentages in the ideal case, in the cases of 25 and 60 μm misalignment in x, y, or z directions, and in the cases of the 100, 200, and 300 μm deep indentations.

Error	$FWHM_E$ (%)	AVE_E (%)	$FWHM_\beta$ (°)	AVE_β (°)	Transm. (%)
Ideal	1.6	0.0	1.4	0.0	4.44
25 μm x shift	1.4	0.0	1.4	0.4	3.95
60 μm x shift	1.3	0.05	1.4	1.1	2.47
25 μm y shift	1.8	0.0	1.4	0.0	4.42
60 μm y shift	3.8	0.0	1.4	0.0	4.42
25 μm z shift	1.5	0.65	1.3	−0.15	4.38
60 μm z shift	1.7	1.65	1.4	−0.3	4.28
100 μm ind.	1.7	−0.05	1.4	0.0	4.39
200 μm ind.	1.7	−0.05	1.5	0.05	4.28
300 μm ind.	1.6	0.0	1.4	0.1	4.12

and the angle β distributions, and the transmission percentages for the misalignments of 25 and 60 μm in each direction are shown in Table II.

The effect of an indentation was studied for a depth parameter ranging from 0 to 600 μm in steps of 25 μm. In each of these cases one million protons were injected, with transmitted particles classified in terms of energy and angles α and β. The 300 μm depth of indentation was chosen for Fig. 5 where the distributions of the energy and angles are shown. An effect similar to the one shown in Fig. 5 was found for each depth. The FWHM values, the average of the energy E and angle β distributions, and the transmission percentages for the 100, 200, and 300 μm deep indentations are shown in Table II.

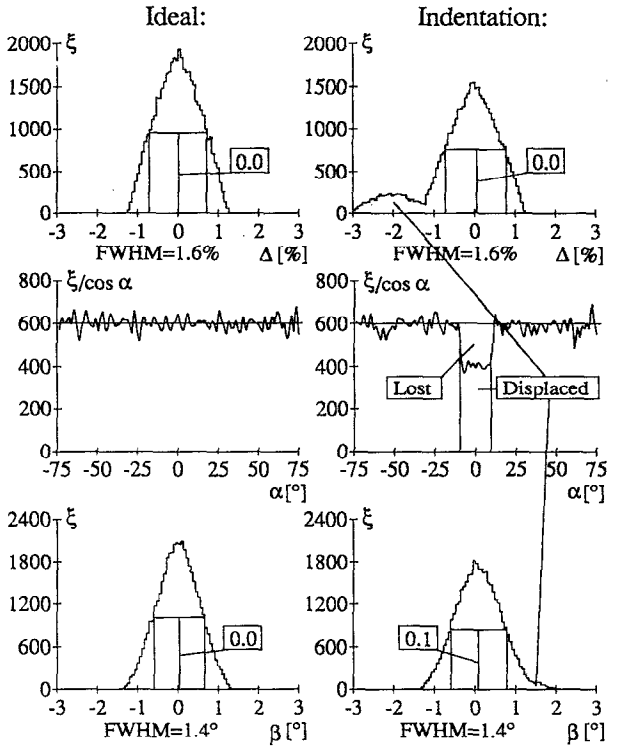

FIG. 5. The energy distributions and the distributions of the angles α and β in an ideal case and in a case when a 300-μm-deep indentation has occurred. The full width at half maximum (FWHM) values and the average of the distributions are shown for the energy and angle β distributions. Particles are lost from the dented area and the remaining ones are displaced both with respect to ideal energy and β spectra. $\Delta=(E-E_0)/E_0$, where E_0 is the nominal kinetic energy. ξ=number of transmitted particles per bin. In the angle α distributions the ξ values are divided by the value of cos α in order that the changes of the distributions become easily perceptible. The bin widths are identical to Fig. 4.

IV. DISCUSSION

Based on these results, a maximum misalignment of 25 μm was specified as an upper limit for the assembly. Within this tolerance the estimated transmission percentage goal can be achieved. As shown in Fig. 3 and Table II, the x direction is the most sensitive to misalignment and therefore special care has to be exercised in aligning the hemispheres in this direction. In the x direction the average of the β distribution shows notable changes but this effect can be taken care of in the calibration process. The alignment in the y direction is also important because of notable changes in energy distributions of the transmitted particles. Figure 4 shows that when a 60 μm misalignment occurs, the FWHM value changes by more than a factor of 2 from its value for the ideal case. The increased FWHM values for energy distributions are still acceptable when the misalignment in the y direction is 25 μm (see Table II). The alignment in the z direction does not give any reason for extra care as it has an effect only on the average of the energy and angle distributions. These effects can easily be taken care of in the calibration process. Figure 4 shows that α distributions do not have any notable changes with 60 μm misalignments. Therefore a maximum misalignment specification of 25 μm is sufficient. Only in the x direction does the α distribution show a notable change, but this effect was already considered in the discussion of transmission percentages.

As a result, a 25 μm error has been specified for each direction. Special care is required in the x and y directions in contrast to the z direction. The 25 μm specification can also be given to geometrical manufacturing errors other than misalignments. Our calculations indicate that generally all geometrical errors have to be limited so that they do not change the analyzer gap width, averaged over the active area, by more than 25 μm.

The indentation does not cause any real reason for extra care as indicated by Fig. 5 and Table II. Figure 5 shows that an indentation causes a loss of particles in the α distributions but these changes can be accounted for in the calibration process. The particles transmitted in the dented area change the energy and β distributions (see Fig. 5). This affect is worse for the FWHM values when the depth of the indentation is between 100 and 200 μm as shown in Table II. The average of the energy and β distributions are also quite unaffected by the indentations as shown in Table II. The loss of particles increases in proportion to the depth of the indentation, but the transmission percentages can still be accepted up to a depth of 300 μm (see Table II).

Indentations used in the calculations have an extension of $\pm 10°$ in the angles α and γ of the inner hemispheres (Fig. 2). However, indentations or elevations that can be expected in manufacturing are typically much smaller than those used in our calculations. In practice the 300 μm value for the depth of the indentation should be considered quite large since an indentation depth of 100 μm could easily be detected mechanically. Therefore, a nominal upper limit of 100 μm can be chosen although our calculations clearly indicate that the hemisphere does not have to be rejected as long as the indentation depth is less than 300 μm.

The final results of the calculations give us confidence that the hemispheres can be manufactured by turning on a lathe, and the expected costs can be kept at reasonable levels. A prototype hemisphere with a 0.4 mm wall thickness and an inner radius of 101.25 mm has been manufactured and the measured shape tolerance was within the range ± 25 μm. The assembly tolerance of the hemispheres has been confirmed to be of the same order of magnitude. The performance of the prototype sensor will be tested using a proton beam during the spring 1993.

ACKNOWLEDGMENTS

The authors would like to acknowledge the Academy of Finland and the Ministry of Trade and Industry for financial support of the project.

[1] NASA, A Proposal for the Plasma Science (PLS) Investigation for the Cassini Orbiter Spacecraft, Volume 1: Investigation and Technical Plan.
[2] S. J. Bame, D. J. McComas, D. T. Young, and R. D. Belian, Rev. Sci. Instrum. **57**, 1711 (1986).
[3] D. J. McComas, J. R. Baldano, S. J. Bame, and B. L. Barraclough, Rev. Sci. Instrum. **58**, 2331 (1987).
[4] M. R. Spiegel, *Theory and Problems of Vector Analysis and an Introduction to Tensor Analysis* (McGraw–Hill, New York, 1959).
[5] I. S. Grant and W. R. Phillips, *Electromagnetism* (Wiley, New York, 1976).
[6] H. Goldstein, *Classical Mechanics*, 2nd edition (Addison–Wesley, London, 1980).
[7] W. H. Press, B. P. Flannery, S. A. Teukolsky, and W. T. Vetterling, Numerical Recipes, *The Art of Scientific Computing* (Cambridge University, Cambridge, 1986).
[8] J. T. Gosling, M. F. Thomsen, and R. C. Anderson, A Cookbook for Determining Essential Transmission Characteristics of Spherical Section Electrostatic Analyzers, Los Alamos National Laboratory, Los Alamos, NM 87545, 1984.